Polymer Journal
https://doi.org/10.1038/s41428-026-01166-5

ORIGINAL ARTICLE

Tikhonov regularization-based reconstruction of partial scattering functions obtained from contrast variation small-angle neutron scattering

Manabu Machida [1] · Koichi Mayumi [2]

Received: 6 November 2025 / Revised: 27 January 2026 / Accepted: 8 February 2026

Abstract

Contrast variation small-angle neutron scattering (CV-SANS) has been widely employed for conducting nano structural analyses of multicomponent systems. In CV-SANS experiments, the scattering intensities of samples with different scattering contrasts are decomposed into partial scattering functions that correspond to the structure of each component and the cross-correlations between different components via singular value decomposition (SVD). However, the estimation of partial scattering functions with small absolute values often suffers from instability due to the significant differences among the singular values. In this paper, we propose a remedy for this instability by introducing Tikhonov regularization, which ensures a more stable reconstruction of the partial scattering functions.

Introduction

Small-angle neutron scattering (SANS) has been used to observe the microscopic structures of materials at the length scale from the nanometer level to the submicrometer level [1]. A unique feature of neutron scattering is that the scattering contrast is drastically changed by the deuteration of material components [1]. SANS with contrast variation via deuteration (CV-SANS) enables nano-structural analyses of multicomponent systems, such as copolymer micelles [2], polymer/inorganic filler composites [3, 4], protein complexes [5] and supramolecular assemblies [6–9].

For example, CV-SANS has been applied to polyrotaxane (PR), a necklace-like supramolecular assembly in which cyclodextrins (CDs) are threaded on a polyethylene glycol (PEG) chain (Fig. 1a) [6–9]. For PR solutions, the scattering intensity $I(Q)$ is given as shown below:

$$I(Q) = \Delta\rho_{\mathrm{C}}^2 S_{\mathrm{CC}}(Q) + \Delta\rho_{\mathrm{P}}^2 S_{\mathrm{PP}}(Q) + 2\Delta\rho_{\mathrm{C}}\Delta\rho_{\mathrm{P}} S_{\mathrm{CP}}(Q), \quad (1)$$

where Q is the magnitude of the scattering vector, $\Delta\rho_i$ is the difference between the scattering length densities (SLDs) of a component i (C: CD or P: PEG) and a solvent, and S_{ij} is a partial scattering function that corresponds to self-correlation ($i = j$) or the cross correlation between different components ($i \neq j$). As shown in Fig. 1a, S_{CC}, S_{PP} and S_{CP} represent the CD structure, the conformation of PEG, and the topological connection between CD and PEG, respectively. In our previous work, the partial scattering functions S_{ij} were determined by a singular value decomposition (SVD) method using the CV-SANS data of PR solutions with different deuteration levels [9]. However, as shown in Fig. 1b, the S_{PP} obtained with the smallest absolute values was noisy. To overcome the instability encountered when determining partial scattering functions, in this work, we apply Tikhonov regularization for the CV-SANS data of the examined PR solutions. This method ensures the stable reconstruction of the partial scattering functions derived from CV-SANS data.

✉ Manabu Machida
machida@hiro.kindai.ac.jp

✉ Koichi Mayumi
kmayumi@issp.u-tokyo.ac.jp

[1] Department of Informatics, Faculty of Engineering, Kindai University, Higashi-Hiroshima, Japan

[2] The Institute for Solid State Physics, The University of Tokyo, Kashiwa-Shi, Japan

Published online: 10 April 2026

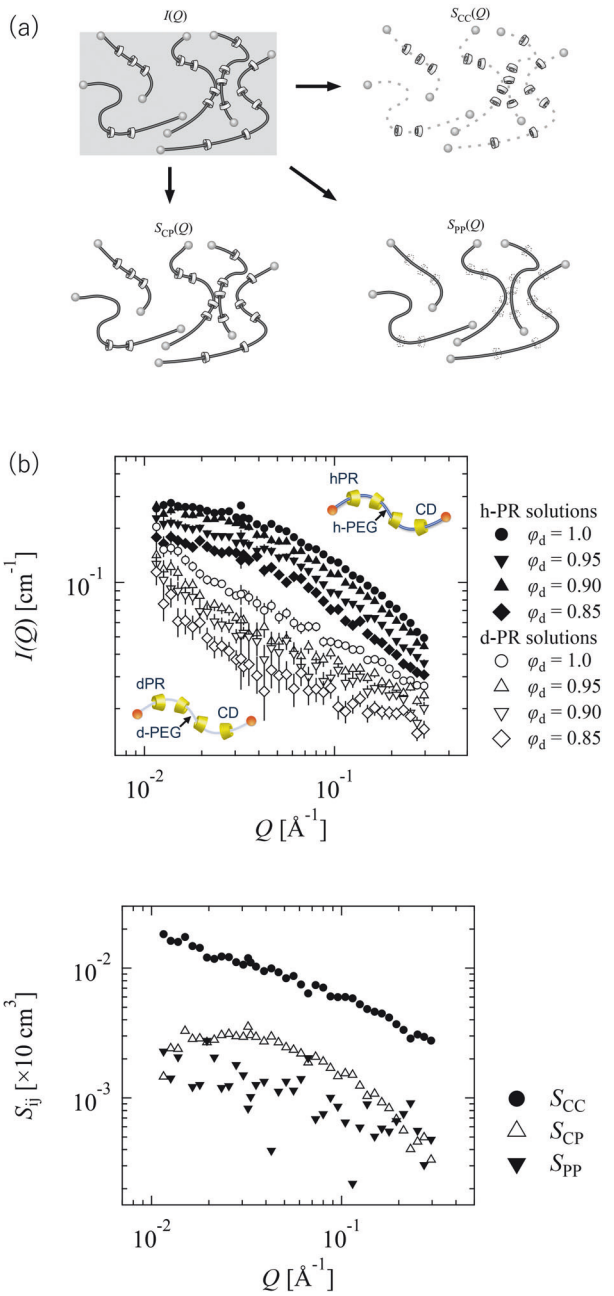

Fig. 1 **a** Schematic illustration of the partial scattering functions S_{ij} of PR solutions. **b** The CV-SANS intensities $I(Q)$ of PR solutions with different deuteration levels and the partial scattering functions $S_{ij}(Q)$ obtained by a singular value decomposition method [6]. Reprinted from Ref. [6] with permission from the American Chemical Society

Methods

CV-SANS experiment involving PR solutions

The CV-SANS data for the evaluated PR solutions were reported in our previous paper [6]. For the CV-SANS measurements of the PR solutions, we used PR consisting of hydrogenated (h-) PEG or deuterated (d-) PEG as a linear polymer chain and α-CDs as rings (Fig. 1b). The scattering length densities ρ of h-PEG, d-PEG and CD were 0.65×10^6, 7.1×10^6 and 2.0×10^6 Å^{-2}, respectively. h-PR and d-PR were dissolved in mixtures of hydrogenated dimethyl sulfoxide (h-DMSO) and deuterated DMSO (d-DMSO). The volume fraction of PR in the solutions was 8%. The volume fractions of d-DMSO in the solvent φ_d were 1.0, 0.95, 0.90 and 0.85, and the corresponding scattering length densities of the solvents were 5.3×10^6, 5.0×10^6, 4.7×10^6 and 4.5×10^6 Å^{-2}, respectively.

The SANS measurements of the PR solutions were performed at 298 K using the SANS-U diffractometer of the Institute for Solid State Physics, The University of Tokyo, which is located at the JRR-3 research reactor of the Japan Atomic Energy Agency in Tokai, Japan. The wavelength of the incident beam was 7.0 Å and the wavelength distribution was 10%. The sample-to-detector distances were 1 and 4 m. The scattered neutrons were collected with a two-dimensional detector. The two-dimensional scattering pattern was converted into a one-dimensional profile via circular averaging. After applying background and cell scattering subtraction, the scattering intensity was normalized to the absolute scattering intensity using a polyethylene film as a standard sample. The corrected scattering intensity I was plotted against Q. The error bar of $I(Q)$ was given by the standard deviation of the circular averaging results.

Inverse problem for determining partial scattering functions from CV-SANS data

We introduce a three-dimensional real vector $\mathbf{S}(Q) = (S_{PP}(Q), S_{CC}(Q), S_{CP}(Q))^T$, where T denotes the transpose of a matrix. Let m be the number of scattering contrasts (we suppose that $m > 3$). That is, we have $I^{(i)}(Q)(i = 1, \ldots, m)$. Then the scattering intensity can be expressed as an m-dimensional real vector $\mathrm{I} = \mathrm{I}(Q)$. Later, we set $m = 8$. From (1), we have

$$\mathbf{I} = A\mathbf{S}, \tag{2}$$

where A is an $m \times 3$ real matrix whose entries can be read from (1).

The above problem (2) can be formulated as the following minimization problem.

$$\begin{aligned} &\operatorname*{gra\,nim}_{\mathbf{S}} \| A\mathbf{S} - \mathbf{I}\|_{\ell^2} \\ &= \operatorname*{gra\,nim}_{S^{(1)},S^{(2)},S^{(3)}} \sqrt{\sum_{i=1}^{m}\left(\sum_{j=1}^{3} A_{ij}S^{(j)} - I^{(i)}\right)^2}. \end{aligned} \tag{3}$$

Since $\mathbf{I}$ is obtained experimentally, the vector contains noise and can be expressed as $\mathbf{I}^\delta$. Let us write

$$\| \mathbf{I}^\delta - \mathbf{I}\|_{\ell^2} \leq \delta, \tag{4}$$

where the constant $\delta > 0$ shows the noise level. We note that $\mathbf{I}$ is given in (2). Below, we will write $\mathbf{I} = A\mathbf{S}_{\text{true}}$, i.e., $\mathbf{S}_{\text{true}}$ is the vector that contains the true partial scattering functions in the medium. In general, I^{δ} does not belong to the range of A and there is no S such that $A\mathbf{S} = \mathbf{I}^{\delta}$. Hence the solution to the minimization problem $\operatorname{gra}\min_{\mathbf{S}} \| A\mathbf{S} - \mathbf{I}^{\delta}\|_{\ell^2}$ might be quite different from the true S.

To remedy this situation, we solve the problem with a suitable regularization [10], and try to find the minimizer S_*:

$$\mathbf{S}_* = \arg\min_{\mathbf{S}} \left(\| A\mathbf{S} - \mathbf{I}^{\delta}\|_{\ell^2}^2 + \alpha^2 \| L\mathbf{S}\|_{\ell^2}^2 \right), \tag{5}$$

where L is a 3×3 matrix and $\alpha > 0$ is a scalar. The second term on the right-hand side of (5) was added to stabilize the solution. In (5), we introduced the diagonal matrix L in addition to the regularization parameter α contained in the penalty term. The reason for this step is that the reconstructed partial scattering functions may have possessed different orders of magnitude. The introduction of L achieved a fair regularization effect.

Let us define

$$\mathbf{s} = L\mathbf{S},\ B = AL^{-1}, \tag{6}$$

and rewrite the minimization problem in (5) as

$$\mathbf{s}_* = \arg\min_{\mathbf{s}} \Phi(\mathbf{s}), \tag{7}$$

where

$$\Phi(\mathbf{s}) = \| B\mathbf{s} - \mathbf{I}^{\delta}\|_{\ell^2}^2 + \alpha^2 \| \mathbf{s}\|_{\ell^2}^2. \tag{8}$$

The solution to (5) is obtained as $\mathbf{S}_* = L^{-1}\mathbf{s}_*$.

Tikhonov regularization

We consider SVD:

$$B = UDV^T, \tag{9}$$

where the $m \times m$ matrix U and 3×3 matrix V are orthogonal matrices, and D is an $m \times 3$ diagonal matrix. The matrix D contains singular values $\mu_j \geq 0$ ($j = 1, 2, 3$), where $\mu_1 \geq \mu_2 \geq \mu_3$. Let λ_j ($j = 1, 2, 3$) be the eigenvalues of B^TB ($\lambda_1 \geq \lambda_2 \geq \lambda_3 \geq 0$). We have the relation stating that $\mu_j = \sqrt{\lambda_j}$ ($j = 1, 2, 3$). We write

$$U = (\cdots \boldsymbol{\psi}_i \cdots),\ V = (\cdots \boldsymbol{\varphi}_k \cdots), \tag{10}$$

where $\boldsymbol{\psi}_i$ is an m-dimensional real vector ($i = 1, \ldots, m$) and $\boldsymbol{\varphi}_k$ is a 3-dimensional real vector ($k = 1, 2, 3$). We note that $\{\boldsymbol{\psi}_i\}$ and $\{\boldsymbol{\varphi}_k\}$ form orthonormal sets. Below, we introduce α, which is the regularization parameter in (5)[10, 11].

Let us define a 3×3 matrix M_α as

$$M_\alpha = \left(\ldots \mathbf{t}_j(\alpha) \cdots \right), \tag{11}$$

where

$$\mathbf{t}_j(\alpha) = \sum_{k=1}^{3} \frac{\varphi_k^{(j)}}{\alpha^2 + \mu_k^2} \boldsymbol{\varphi}_k, \quad j = 1, 2, 3. \tag{12}$$

We have that

$$\begin{aligned} (\alpha^2 E + B^TB)M_\alpha &= \alpha^2 M_\alpha + B^TBM_\alpha \\ &= (\cdots \alpha^2 \mathbf{t}_j(\alpha) \cdots) + (\cdots B^TB\mathbf{t}_j(\alpha) \cdots), \end{aligned} \tag{13}$$

where $E \in \mathbf{R}^{3\times 3}$ is the identity. Since

$$\begin{aligned} \left\{B^TB\mathbf{t}_j(\alpha)\right\}_i &= \left\{VD^TDV^T\mathbf{t}_j(\alpha)\right\}_i \\ &= \sum_{k=1}^{3} \frac{\mu_k^2}{\alpha^2 + \mu_k^2} \varphi_k^{(i)} \varphi_k^{(j)} \end{aligned} \tag{14}$$

for $i = 1, 2, 3$, we obtain

$$\left\{\alpha^2 \mathbf{t}_j(\alpha) + B^TB\mathbf{t}_j(\alpha)\right\}_i = \sum_{k=1}^{3} \varphi_k^{(i)} \varphi_k^{(j)}. \tag{15}$$

Hence,

$$\left(\alpha^2 E + B^TB\right)M_\alpha = VV^T = E. \tag{16}$$

Similarly,

$$M_\alpha\left(\alpha^2 + B^TB\right) = E. \tag{17}$$

Equations (16) and (17) yield

$$M_\alpha = \left(\alpha^2 + B^TB\right)^{-1}. \tag{18}$$

Hence, the matrix $\alpha^2 + B^TB$ is invertible.

Let us define a matrix B_{reg}^{+} as

$$B_{\text{reg}}^{+} = \left(\alpha^2 + B^TB\right)^{-1} B^T. \tag{19}$$

This B_{reg}^{+} is a regularized Moore–Penrose pseudoinverse. We note that the Moore–Penrose pseudoinverse of B is wirtten as $B^{+} = (B^TB)^{-1}B^T = V(D^TD)^{-1}D^TU^T$.

Next we consider how B_{reg}^{+} can be used to obtain $\mathbf{s}_*$. Let $\mathbf{s}_\alpha^{\delta}$ be the solution of

$$\alpha^2 \mathbf{s}_\alpha^{\delta} + B^TB\mathbf{s}_\alpha^{\delta} = B^T\mathbf{I}^{\delta}. \tag{20}$$

For any 3-dimensional real vector $\mathbf{s}$, we have that

$$\begin{aligned}
&\| B\mathbf{s} - \mathbf{I}^\delta\|_{\ell^2}^2 + \alpha^2 \| \mathbf{s}\|_{\ell^2}^2 \\
&= \| B\mathbf{s}_\alpha^\delta - \mathbf{I}^\delta\|_{\ell^2}^2 + \alpha^2 \| \mathbf{s}_\alpha^\delta\|_{\ell^2}^2 \\
&\quad + 2(\mathbf{s} - \mathbf{s}_\alpha^\delta) \cdot \left(\alpha^2 \mathbf{s}_\alpha^\delta + B^T(B\mathbf{s}_\alpha^\delta - \mathbf{I}^\delta)\right) \\
&\quad + \| B(\mathbf{s} - \mathbf{s}_\alpha^\delta)\|_{\ell^2}^2 + \alpha^2 \| \mathbf{s} - \mathbf{s}_\alpha^\delta\|_{\ell^2}^2 \\
&= \| B\mathbf{s}_\alpha^\delta - \mathbf{I}^\delta\|_{\ell^2}^2 + \alpha^2 \| \mathbf{s}_\alpha^\delta\|_{\ell^2}^2 + \| B(\mathbf{s} - \mathbf{s}_\alpha^\delta)\|_{\ell^2}^2 \\
&\quad + \alpha^2 \| \mathbf{s} - \mathbf{s}_\alpha^\delta\|_{\ell^2}^2.
\end{aligned} \tag{21}$$

This means that for $\alpha > 0$, there exists a unique $\mathbf{s}_\alpha^\delta$ such that

$$\Phi(\mathbf{s}_\alpha^\delta) = \inf_{\mathbf{s}} \Phi(\mathbf{s}). \tag{22}$$

Due to the fact that $\nabla\Phi = (\partial\Phi/\partial s^{(1)}, \partial\Phi/\partial s^{(2)}, \partial\Phi/\partial s^{(3)})^T = 2B^T(B\mathbf{s} - \mathbf{I}^\delta) + 2\alpha^2\mathbf{s} = 0$, we observe that (20) is necessary and sufficient for $\mathbf{s}_\alpha^\delta$ to minimize the Tikhonov functional (22). Thus, $\mathbf{s}_*$ can be computed as (recall (8))

$$\mathbf{s}_* = \mathbf{s}_\alpha^\delta = B_{\mathrm{reg}}^+ \mathbf{I}^\delta. \tag{23}$$

We note that both $\mathbf{s}_*$ and B_{reg}^+ depend on α.

We can write the following:

$$\begin{aligned}
\mathbf{s}_* &= (\alpha^2 E + B^T B)^{-1} B^T \mathbf{I}^\delta \\
&= MVD^T U^T \mathbf{I}^\delta \\
&= \sum_{k=1}^{3} \frac{1}{\alpha^2 + \mu_k^2} \boldsymbol{\varphi}_k \sum_{i=1}^{3}\sum_{j=1}^{3} \varphi_k^{(i)} \varphi_j^{(i)} \mu_j' \boldsymbol{\psi}_j \mathbf{I}^\delta \\
&= \sum_{k=1}^{3} \frac{\mu_k}{\alpha^2 + \mu_k^2} (\boldsymbol{\psi}_k \cdot \mathbf{I}^\delta) \boldsymbol{\varphi}_k \\
&= \sum_{k=1}^{3} \frac{1}{\mu_k} q(\alpha, \mu_k) (\boldsymbol{\psi}_k \cdot \mathbf{I}^\delta) \boldsymbol{\varphi}_k,
\end{aligned} \tag{24}$$

where

$$q(\alpha, \mu) = \frac{\mu^2}{\alpha^2 + \mu^2}. \tag{25}$$

We note that $0 < q(\alpha, \mu) < 1$ and $q(\alpha, \mu) \leq \mu/(2\alpha)$ because

$$\frac{1}{2\alpha} - \frac{\mu}{\alpha^2 + \mu^2} = \frac{(\alpha - \mu)^2}{2\alpha(\alpha^2 + \mu^2)} \geq 0. \tag{26}$$

The Tikhonov filter $q(\alpha, \mu)$ is close to 1 when $\alpha \ll \mu$ and is close to 0 when $\alpha \gg \mu$. Thus, roughly speaking, α controls how many SVD components are included in $\mathbf{s}_*$.

Let us estimate the error of the obtained solution $\mathbf{s}_*$. Let $\mu_{n_0} > 0$ be the smallest nonzero singular value. We have the following:

$$\begin{aligned}
\| \mathbf{s}_* - B_{\mathrm{reg}}^+ \mathbf{I}\|_{\ell^2} &= \| B_{\mathrm{reg}}^+ \mathbf{I}^\delta - B_{\mathrm{reg}}^+ \mathbf{I}\|_{\ell^2} \\
&= \left\| \sum_{k=1}^{3} \frac{1}{\mu_k} q(\alpha, \mu_k) (\boldsymbol{\psi}_k \cdot (\mathbf{I}^\delta - \mathbf{I})) \boldsymbol{\varphi}_k \right\|_{\ell^2} \\
&\leq \min\left(\frac{1}{2\alpha}, \frac{1}{\mu_{n_0}}\right) \left\| \sum_{k=1}^{3} (\boldsymbol{\psi}_k \cdot (\mathbf{I}^\delta - \mathbf{I})) \boldsymbol{\varphi}_k \right\|_{\ell^2} \\
&= \min\left(\frac{1}{2\alpha}, \frac{1}{\mu_{n_0}}\right) \left(\sum_{k=1}^{3} \left| \boldsymbol{\psi}_k \cdot (\mathbf{I}^\delta - \mathbf{I}) \right|^2 \right)^{1/2} \\
&\leq \min\left(\frac{1}{2\alpha}, \frac{1}{\mu_{n_0}}\right) \| \mathbf{I}^\delta - \mathbf{I}\|_{\ell^2} \\
&\leq \min\left(\frac{1}{2\alpha}, \frac{1}{\mu_{n_0}}\right) \delta.
\end{aligned} \tag{27}$$

We note that $\mathrm{I} = B\mathbf{s}_{\mathrm{true}}$, where $\mathrm{s}_{\mathrm{true}} = L\mathrm{S}_{\mathrm{true}}$. Since $\| \mathbf{s}_* - \mathbf{s}_{\mathrm{true}}\|_{\ell^2} \leq \| \mathbf{s}_* - B_{\mathrm{reg}}^+ \mathbf{I}\|_{\ell^2} + \| B_{\mathrm{reg}}^+ \mathbf{I} - \mathbf{s}_{\mathrm{true}}\|_{\ell^2}$, the following inequality holds.

$$\begin{aligned}
\| \mathbf{s}_* - \mathbf{s}_{\mathrm{true}}\|_{\ell^2} \leq \min\left(\frac{1}{2\alpha}, \frac{1}{\mu_{n_0}}\right) \delta \\
+ \| B_{\mathrm{reg}}^+ B\mathbf{s}_{\mathrm{true}} - \mathbf{s}_{\mathrm{true}}\|_{\ell^2}.
\end{aligned} \tag{28}$$

The right-hand side of (28) implies that we can set $\alpha = 0$ if δ/μ_{n_0} is sufficiently small. Otherwise, if $\alpha = 0$ (no regularization) and μ_{n_0} is small, (28) means that the reconstructed $\mathbf{s}_*$ might be significantly different from $\mathbf{s}_{\mathrm{true}}$. When δ is large or μ_{n_0} is small, however, a better solution can be obtained with a finite $\alpha > 0$.

Due to the use of regularization, even in the ideal case with no noise, the reconstructed $\mathbf{s}_*$ differs from $\mathbf{s}_{\mathrm{true}}$. Let us write

$$\mathbf{s}_{\mathrm{proj}} = B_{\mathrm{reg}}^+ B\mathbf{s}_{\mathrm{true}}. \tag{29}$$

This $\mathbf{s}_{\mathrm{proj}}$ is the best result that we can obtain. We note that (29) can be rewritten as

$$\begin{aligned}
\mathbf{s}_{\mathrm{proj}} &= \left(\alpha^2 + B^T B\right)^{-1} B^T B\mathbf{s}_{\mathrm{true}} \\
&= \mathbf{s}_{\mathrm{true}} - \alpha^2 M_\alpha \mathbf{s}_{\mathrm{true}}.
\end{aligned} \tag{30}$$

where the Woodbury formula was used. Equation (30) explains that $\mathbf{s}_{\mathrm{proj}}$ does not match $\mathbf{s}_{\mathrm{true}}$ by the introduction of $\alpha > 0$.

To deepen the understanding of regularization, let us write

$$\| B\mathbf{s} - \mathbf{I}^\delta\|_{\ell^2}^2 + \alpha^2 \| \mathbf{s}\|_{\ell^2}^2 = \left\| \widetilde{B}_\alpha \mathbf{s} - \begin{pmatrix} \mathbf{I}^\delta \\ \mathbf{0} \end{pmatrix} \right\|_{\ell^2}^2, \tag{31}$$

where $\mathbf{0} = (0\,0\,0)^T$ and

$$\widetilde{B}_\alpha = \begin{pmatrix} B \\ \alpha E \end{pmatrix}. \tag{32}$$

We have that

$$\mathbf{s}_\alpha^\delta = B_{\mathrm{reg}}^+ \mathbf{I}^\delta = \widetilde{B}_\alpha^+ \begin{pmatrix} \mathbf{I}^\delta \\ \mathbf{0} \end{pmatrix}, \tag{33}$$

where

$$\widetilde{B}_\alpha^+ = \left(\widetilde{B}_\alpha^T \widetilde{B}_\alpha\right)^{-1} \widetilde{B}_\alpha^T. \tag{34}$$

Let us introduce the orthogonal projection matrix $P_\alpha \in \mathrm{R}^{(m+1)\times(m+1)}$ as shown below:

$$P_\alpha = \widetilde{B}_\alpha \widetilde{B}_\alpha^+. \tag{35}$$

Indeed, through direct calculations, we can show that $P_\alpha^T = P_\alpha$ and $P_\alpha^2 = P_\alpha$. We have already seen that $B\mathbf{s}_\alpha^\delta$ is different from I^δ. The former vector satisfies the following equality:

$$\widetilde{B}_\alpha \mathbf{s}_\alpha^\delta = P_\alpha \begin{pmatrix} \mathbf{I}^\delta \\ \mathbf{0} \end{pmatrix}. \tag{36}$$

This means that in the $(m+1)$-dimensional space, we take only a *good* subspace into account to obtain $\mathbf{s}_\alpha^\delta$. The cost function (8) can be calculated as

$$\begin{aligned} \Phi(\mathbf{s}_\alpha^\delta) &= \left\| \begin{pmatrix} \mathbf{I}^\delta \\ \mathbf{0} \end{pmatrix} - P_\alpha \begin{pmatrix} \mathbf{I}^\delta \\ \mathbf{0} \end{pmatrix} \right\|_{\ell^2}^2 \\ &= \|\mathbf{I}^\delta\|_{\ell^2}^2 - \left\| P_\alpha \begin{pmatrix} \mathbf{I}^\delta \\ \mathbf{0} \end{pmatrix} \right\|_{\ell^2}^2. \end{aligned} \tag{37}$$

In general, $\Phi(\mathbf{s}_\alpha^\delta)$ reaches its minimum value with a nonzero α. To see the relation shown in (37), we note that

$$\begin{aligned} \left\| \begin{pmatrix} \mathbf{I}^\delta \\ \mathbf{0} \end{pmatrix} \right\|_{\ell^2}^2 &= \left\| P_\alpha \begin{pmatrix} \mathbf{I}^\delta \\ \mathbf{0} \end{pmatrix} + \begin{pmatrix} \mathbf{I}^\delta \\ \mathbf{0} \end{pmatrix} - P_\alpha \begin{pmatrix} \mathbf{I}^\delta \\ \mathbf{0} \end{pmatrix} \right\|_{\ell^2}^2 \\ &= \left\| P_\alpha \begin{pmatrix} \mathbf{I}^\delta \\ \mathbf{0} \end{pmatrix} \right\|_{\ell^2}^2 + \left\| \begin{pmatrix} \mathbf{I}^\delta \\ \mathbf{0} \end{pmatrix} - P_\alpha \begin{pmatrix} \mathbf{I}^\delta \\ \mathbf{0} \end{pmatrix} \right\|_{\ell^2}^2 \\ &\quad + 2P_\alpha \begin{pmatrix} \mathbf{I}^\delta \\ \mathbf{0} \end{pmatrix} \cdot \left[\begin{pmatrix} \mathbf{I}^\delta \\ \mathbf{0} \end{pmatrix} - P_\alpha \begin{pmatrix} \mathbf{I}^\delta \\ \mathbf{0} \end{pmatrix} \right]. \end{aligned} \tag{38}$$

The last term on the right-hand side vanishes:

$$\begin{aligned} & P_\alpha \begin{pmatrix} \mathbf{I}^\delta \\ \mathbf{0} \end{pmatrix} \cdot \left[\begin{pmatrix} \mathbf{I}^\delta \\ \mathbf{0} \end{pmatrix} - P_\alpha \begin{pmatrix} \mathbf{I}^\delta \\ \mathbf{0} \end{pmatrix} \right] \\ &= \begin{pmatrix} \mathbf{I}^\delta \\ \mathbf{0} \end{pmatrix}^T P_\alpha^T \left[\begin{pmatrix} \mathbf{I}^\delta \\ \mathbf{0} \end{pmatrix} - P_\alpha \begin{pmatrix} \mathbf{I}^\delta \\ \mathbf{0} \end{pmatrix} \right] \\ &= \begin{pmatrix} \mathbf{I}^\delta \\ \mathbf{0} \end{pmatrix}^T \left[P_\alpha \begin{pmatrix} \mathbf{I}^\delta \\ \mathbf{0} \end{pmatrix} - P_\alpha^2 \begin{pmatrix} \mathbf{I}^\delta \\ \mathbf{0} \end{pmatrix} \right] \\ &= 0. \end{aligned} \tag{39}$$

Reconstruction quality

Let us set

$$x = \ln Q,\ y = \ln S^{(j)}\ (j = 1, 2, 3). \tag{40}$$

We can evaluate the fluctuation exhibited by the reconstruction result by calculating the typical distance from (x, y) to the principal axis.

Suppose that Q is discretized as Q_i $(i = 1, \ldots, N_Q)$ and that x, y are discretized into N_Q points x_i, y_i $(i = 1, \ldots, N_Q)$. The averages $\overline{x}, \overline{y}$ are computed as

$$\overline{x} = \frac{1}{N_Q} \sum_{i=1}^{N_Q} x_i,\ \overline{y} = \frac{1}{N_Q} \sum_{i=1}^{N_Q} y_i. \tag{41}$$

We introduce a real matrix $Z \in \mathbb{R}^{N\times 2}$. The elements of Z are given by

$$Z_{1i} = x_i - \overline{x},\ Z_{2i} = y_i - \overline{y} \tag{42}$$

for $i = 1, \ldots, N_Q$. We define

$$\Sigma = \begin{pmatrix} \frac{1}{N_Q} \sum_{i=1}^{N_Q} Z_{1i}^2 & \frac{1}{N_Q} \sum_{j=1}^{N_Q} Z_{1i} Z_{2i} \\ \frac{1}{N_Q} \sum_{i=1}^{N_Q} Z_{2i} Z_{1i} & \frac{1}{N_Q} \sum_{i=1}^{N_Q} Z_{2i}^2 \end{pmatrix}. \tag{43}$$

Let λ_1, λ_2 be the largest and second-largest eigenvalues of Σ, respectively. Let $\mathrm{v}^{(1)}$, $\mathrm{v}^{(2)}$ $(|\mathrm{v}^{(1)}| = |\mathrm{v}^{(2)}| = 1)$ be the eigenvectors that correspond to λ_1, λ_2, respectively. We can write

$$\Sigma = (\mathbf{v}^{(1)}\, \mathbf{v}^{(2)}) \begin{pmatrix} \lambda_1 & 0 \\ 0 & \lambda_2 \end{pmatrix} (\mathbf{v}^{(1)} \mathbf{v}^{(2)})^T. \tag{44}$$

Let $\mathrm{p}^{(i)}$ be a two-dimensional vector ($i = 1, \ldots, N_Q$):

$$\mathbf{p}^{(i)} = \begin{pmatrix} x_i \\ y_i \end{pmatrix}. \tag{45}$$

The projection of $\mathrm{p}^{(i)}$ in the direction of a unit vector v ($|\mathrm{v}| = 1$) is given by $\mathrm{v} \cdot \mathrm{p}^{(i)}$. The variance of the projected points is

$$\frac{1}{N_Q}\sum_{i=1}^{N_Q}\left(\mathbf{v}\cdot\begin{pmatrix} Z_{1i} \\ Z_{2i}\end{pmatrix}\right)^2 = \mathbf{v}^T\left(\frac{1}{N_Q}\sum_{i=1}^{N_Q}\begin{pmatrix} Z_{1i} \\ Z_{2i}\end{pmatrix}\begin{pmatrix} Z_{1i} \\ Z_{2i}\end{pmatrix}^T\right)\mathbf{v} = \mathbf{v}^T\Sigma\mathbf{v} = \lambda_1\left(\mathbf{v}\cdot\mathbf{v}^{(1)}\right)^2 + \lambda_2\left(\mathbf{v}\cdot\mathbf{v}^{(2)}\right)^2. \tag{46}$$

Hence, the variance takes its maximum value λ_1 when $\mathrm{v} = \mathrm{v}^{(1)}$.

Since the vector $\mathbf{v}^{(1)}$ is a unit vector along the principal axis and $\mathbf{v}^{(2)}$ is perpendicular to this axis, we can write the principal and second principal components as

$$X_i = \mathbf{v}^{(1)}\cdot\mathbf{p}^{(i)},\ Y_i = \mathbf{v}^{(2)}\cdot\mathbf{p}^{(i)},\ i = 1, \ldots, N_Q. \tag{47}$$

Then we can compute the standard deviation σ as

$$\sigma = \left(\frac{1}{N_Q}\sum_{j=1}^{N_Q}(Y_i - \overline{Y})^2\right)^{1/2},\ \overline{Y} = \frac{1}{N_Q}\sum_{i=1}^{N_Q} Y_i. \tag{48}$$

We note that σ is small if the $S^{(j)}(Q_i)$ are aligned in the direction of the principal axis and σ is large if the plot is rough.

Results and discussion

Numerical tests

In this section we test our inverse algorithm using numerically calculated forward data I^{δ}. According to Ref. [6], we set $m = 8$. We take N_Q values of Q (Q_i, $i = 1, \ldots, N_Q$), where $N_Q = 39$. As shown in (1) and (2), each row of A has $\Delta\rho_{\mathrm{P}}^2$, $\Delta\rho_{\mathrm{C}}^2$ and $2\Delta\rho_{\mathrm{C}}\Delta\rho_{\mathrm{P}}$. Let us use the matrix A which was also used in Ref. [6]:

$A_{11} = 21.2652051242863,$

$A_{12} = 10.8267092340648,$

$A_{13} = 30.3808246232,$

$A_{21} = 18.8919928157135,$

$A_{22} = 9.15345279381885,$

$A_{23} = 26.3003394974132,$

$A_{31} = 16.6591554144896,$

$A_{32} = 7.62057126092164,$

$A_{33} = 22.5346205632921,$

$A_{41} = 14.5666929206144,$

$A_{42} = 6.22806463537323,$

$A_{43} = 19.0496514438685,$

$A_{51} = 3.54675562126379,$

$A_{52} = 10.8267092340648,$

$A_{53} = -12.3934969779652,$

$A_{61} = 4.61481630508689,$

$A_{62} = 9.15345279381885,$

$A_{63} = -12.9986927343881,$

$A_{71} = 5.82325189625878,$

$A_{72} = 7.62057126092164,$

$A_{73} = -13.3231386761134,$

$A_{81} = 7.17206239477945,$

$A_{82} = 6.22806463537323,$

$A_{83} = -13.3668348031411.$

Singular values of A are obtained as $\mu_1 = 64.836$, $\mu_2 = 30.846$ and $\mu_3 = 4.5481$. In this numerical test, we suppose that $\mathbf{S}(Q) = (S_{\mathrm{PP}}(Q), S_{\mathrm{CC}}(Q), S_{\mathrm{CP}}(Q))^T$ is given by

$$S_{\mathrm{PP}}(Q) = \frac{e^{-9}}{\sqrt{Q}},$$

$$S_{\mathrm{CC}}(Q) = \frac{e^{-6}}{\sqrt{Q}},$$

$$S_{\mathrm{CP}}(Q) = \frac{e^{-8}}{\sqrt{Q}}.$$

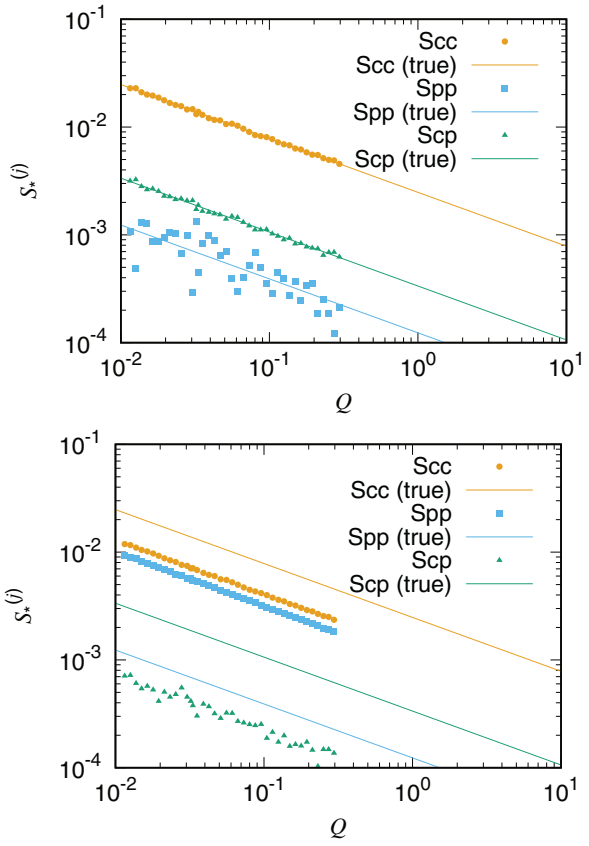

Fig. 2 The regularization matrix is set to $L = E$. The regularization parameter is set to (top) $\alpha = 0$ (no regularization) and (bottom) $\alpha = 10$. Here, $S_*^{(1)} = S_{\mathrm{PP},*}$, $S_*^{(2)} = S_{\mathrm{CC},*}$ and $S_*^{(3)} = S_{\mathrm{CP},*}$

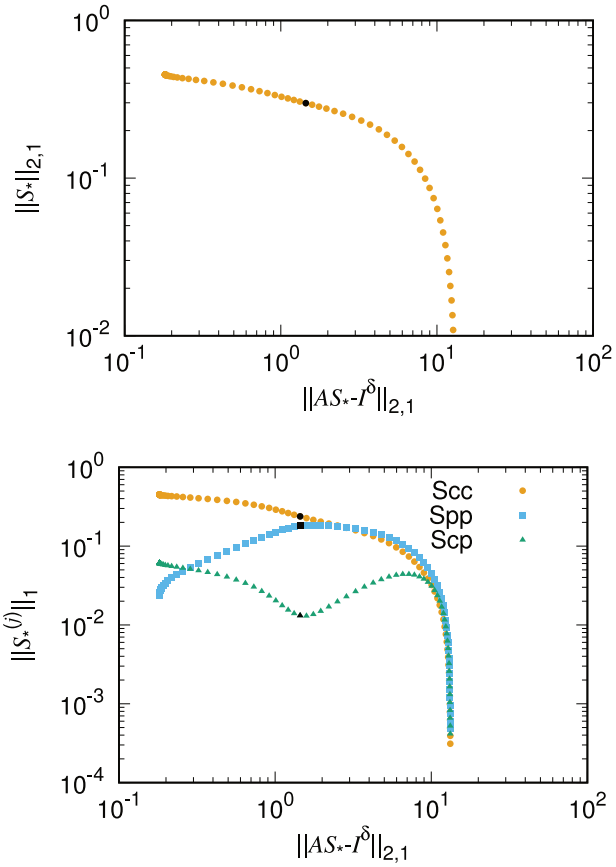

Fig. 3 $L = E$. Here, $S_*^{(1)} = S_{\mathrm{PP},*}$, $S_*^{(2)} = S_{\mathrm{CC},*}$ and $S_*^{(3)} = S_{\mathrm{CP},*}$

Furthermore, we prepare experimental data $\mathbf{I}^\delta$ by adding 3% noise to $\mathbf{I} = A\mathbf{S}$ using uniformly distributed pseudorandom numbers. We express the components of $\mathbf{S}_*$ as $S_*^{(1)}(Q) = S_{\mathrm{PP},*}(Q)$, $S_*^{(2)}(Q) = S_{\mathrm{CC},*}(Q)$ and $S_*^{(3)}(Q) = S_{\mathrm{CP},*}(Q)$.

First, let us set $L = E$ and $\alpha = 0$ (no regularization). By using (23), we obtain $\mathbf{S}_* = \mathbf{s}_* = B^+\mathbf{I}^\delta = A^+\mathbf{I}^\delta$. The result is shown in Fig. 2 (top). Although the reconstructed S_{CC} and S_{CP} are accurate, the reconstructed S_{PP}, which is the smallest component of $\mathbf{S}_*$ is unstable.

Next, we perform regularization and set $\alpha = 10$ while keeping $L = E$, i.e., $\mathbf{S}_* = A^+_{\mathrm{reg}}\mathbf{I}^\delta$ ($A^+_{\mathrm{reg}} = B^+_{\mathrm{reg}}$ in this case). The results are shown in Fig. 2 (bottom). In this case, the reconstructed $\mathbf{S}_*$ is different from the true $\mathbf{S}$. Roughly speaking, we ignore the smallest singular value μ_3 by setting $\alpha = 10$. We note that $q(\alpha, \mu_3)$ is small relative to $q(\alpha, \mu_1)$ and $q(\alpha, \mu_2)$.

Let us introduce the following notations:

$$\| \mathbf{S}_* \|_{2,1} = \sum_{i=1}^{N_Q} \sqrt{\sum_{j=1}^{3} \left(S_*^{(j)}(Q_i)\right)^2}, \tag{49}$$

$$\| S_*^{(j)} \|_1 = \sum_{i=1}^{N_Q} |S_*^{(j)}(Q_i)|, \tag{50}$$

and

$$\| A\mathbf{S}_* - \mathbf{I}^\delta \|_{2,1} = \sum_{i=1}^{N_Q} \| A\mathbf{S}_*(Q_i) - \mathbf{I}^\delta(Q_i) \|_{\ell^2}. \tag{51}$$

In Fig. 3, we plot (top) $\|\mathbf{S}_*\|_{2,1}$ and (bottom) $\|S_{\mathrm{PP},*}\|_1$, $\|S_{\mathrm{CC},*}\|_1$, and $\|S_{\mathrm{CP},*}\|_1$ against $\|A\mathbf{S}_* - \mathbf{I}^\delta\|_{2,1}$ for different values of α. In both panels of Fig. 3, the points for $\alpha = 10$ are shown in black. On all curves contained in Fig. 3, the points move to the right ($\|A\mathbf{S}_* - \mathbf{I}^\delta\|_{2,1}$ becomes larger) as α increases. Figure 3 (bottom) shows that it is impossible to simultaneously perform suitable regularization simultaneously for all S_{PP}, S_{CC}, S_{CP} because α being smaller than 10 makes $\|S_{\mathrm{PP},*}\|_1$ smaller than the value for $\alpha = 10$ but makes $\|S_{\mathrm{CC},*}\|_1$ and $\|S_{\mathrm{CP},*}\|_1$ larger. In the spirit of the L-curve method [12], we compare two terms included in the cost function (see (5)) and plot $\|\mathbf{S}_*\|_{2,1}$ and $\| S_*^{(j)} \|_1$ against $\| A\mathbf{S} - \mathbf{I}^\delta \|^2_{\ell^2}$. The left edge of a curve in Fig. 3 corresponds to the corner of the alphabet L.

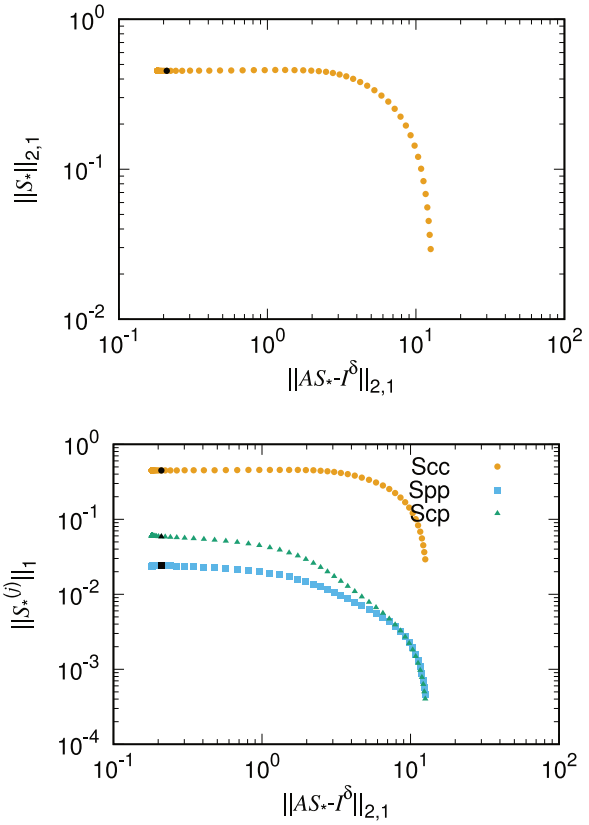

Fig. 4 $L_1 = 1$, $L_2 = 0.1$, $L_3 = 1$. Here, $S_*^{(1)} = S_{\mathrm{PP},*}$, $S_*^{(2)} = S_{\mathrm{CC},*}$ and $S_*^{(3)} = S_{\mathrm{CP},*}$

To improve the reconstruction procedure, let us set the matrix L as a diagonal matrix $L = \mathrm{diag}(L_1, L_2, L_3)$ with $L_1 = 1, L_2 = 0.1, L_3 = 1$. Since the second component $S_{\mathrm{CC},*}$ of $\mathbf{S}_*$ is the largest (see Fig. 2), we can achieve a fair regularization by setting L_2 smaller than L_1, L_3. Indeed, the true S_{CC} is significantly larger than the true S_{PP}, S_{CP}.

We set $\alpha = 10$ with the above-mentioned diagonal matrix L. In Fig. 4, we plot (top) $\|\mathbf{S}_*\|_{2,1}$ and (bottom) $\|S_{\mathrm{PP},*}\|_1$, $\|S_{\mathrm{CC},*}\|_1$, and $\|S_{\mathrm{CP},*}\|_1$ against $\|A\mathbf{S}_* - \mathbf{I}^\delta\|_{2,1}$ for different values of α. The points for $\alpha = 10$ are shown in black. In this case, the curves change monotonically (the points in both panels of Fig. 4 move to the left when α decreases.), and a suitable regularization is achieved for all S_{PP}, S_{CC}, S_{CP}. The reconstructed $\mathbf{S}_*$ is shown in Fig. 5.

To see how the reconstruction procedure is affected by noise, we repeat the above reconstruction process (Fig. 5) for $\mathbf{I}^\delta$ with 1, 5, 10% noise, as shown in Fig. 6. The reconstruction results are more precise if the noise in $\mathbf{I}^\delta$ is smaller.

Reconstruction results obtained for the experimental CV-SANS data of the PR solution

Let us consider the experimental CV-SANS data of the PR solution described in Ref. [6]. The matrix A was given

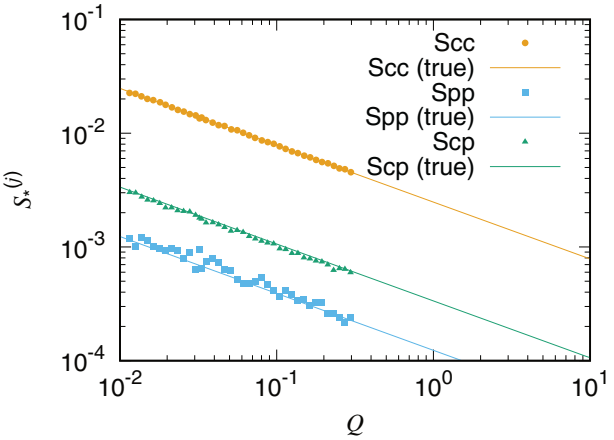

Fig. 5 The reconstruction for $L_1 = 1$, $L_2 = 0.1$, $L_3 = 1$ and $\alpha = 10$. Here, $S_*^{(1)} = S_{\mathrm{PP},*}$, $S_*^{(2)} = S_{\mathrm{CC},*}$ and $S_*^{(3)} = S_{\mathrm{CP},*}$

above, and we set $m = 8$ and $N_Q = 39$. We use the diagonal matrix L that was employed in the previous section: $L = \mathrm{diag}(1, 0.1, 1)$. This means that a weak regularization is performed for S_{CC}.

To choose $\alpha > 0$, we plotted $\|\mathbf{S}_*\|_{2,1}$ and $\|S_*^{(j)}\|_1$ $(j = 1, 2, 3)$ as functions of $\|A\mathbf{S}_* - \mathbf{I}^\delta\|_{2,1}$ in Fig. 7 by reconstructing $S_{\mathrm{CC},*}$, $S_{\mathrm{PP},*}$ and $S_{\mathrm{CP},*}$ for different values of α. The points obtained for $\alpha = 10$ are shown in black in Fig. 7.

The upper panel of Fig. 8 corresponds to Fig. 4 of Ref. [6] and shows the reconstructed $S_{\mathrm{CC},*}$, $S_{\mathrm{CP},*}$, $S_{\mathrm{PP},*}$ as functions of Q. The reconstructed results produced with regularization are shown in the lower panel of Fig. 8. These curves are more stably obtained.

In Fig. 8, we obtained $\sigma = 0.704$ (see Sec. 2.4) for $S_*^{(1)} = S_{\mathrm{PP}}$ with $\alpha = 0$ (no regularization) and acquire $\sigma = 0.197$ for $_*(1) = S_{\mathrm{PP}}$ with $\alpha = 10$ and $L = \mathrm{diag}(1, 0.1, 1)$. Thus, the proposed regularization suppresses fluctuations in the naive reconstruction, and we can quantitatively confirm the effect of regularization.

We note that the number of contrast conditions can be less than 8 ($m < 8$). Moreover, the condition number (the ratio of the largest singular value to the smallest singular value) of A should not be extremely large despite the fact the proposed regularization method suppresses instability caused by large condition numbers. To see this situation, let us look at the following 3×3 matrices $A^{(123)}$ and $A^{(456)}$:

$$A_{i,j}^{(123)} = A_{ij}\,(i = 1,2,3,\, j = 1,2,3),\ A_{i-3,j}^{(456)} = A_{ij}\,(i = 4,5,6,\, j = 1,2,3). \tag{52}$$

The upper three lines (h-PR solutions: $\varphi_{\mathrm{d}} = 1.0, 0.95, 0.90$) in Fig. 1b are used for $A^{(123)}$, and the 4th, 5th, and 6th lines (h-PR solution: $\varphi_{\mathrm{d}} = 0.85$, d-PR solutions: $\varphi_{\mathrm{d}} = 1.0, 0.95$) are used for $A^{(456)}$. The condition numbers of $A^{(123)}$, $A^{(456)}$ are 1.45×10^3 and 19.2, respectively. As shown in

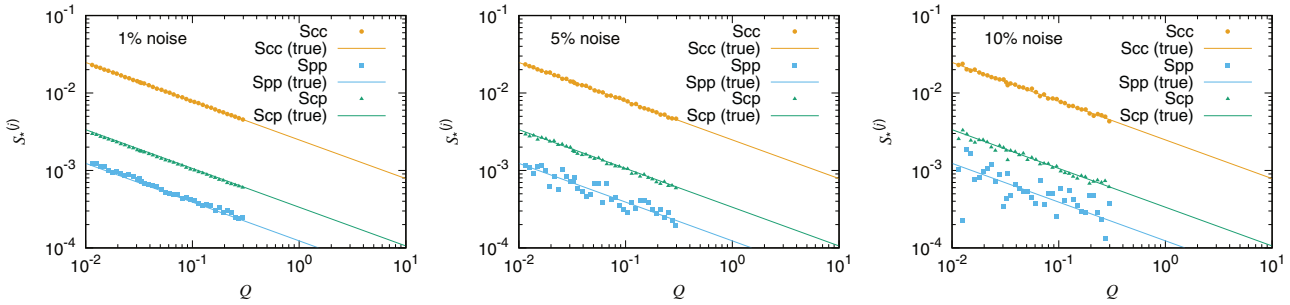

Fig. 6 Same as Fig. 5 (3% noise) but the noise level of the forward data were (Left) 1%, (Center) 5%, and (Right) 10%

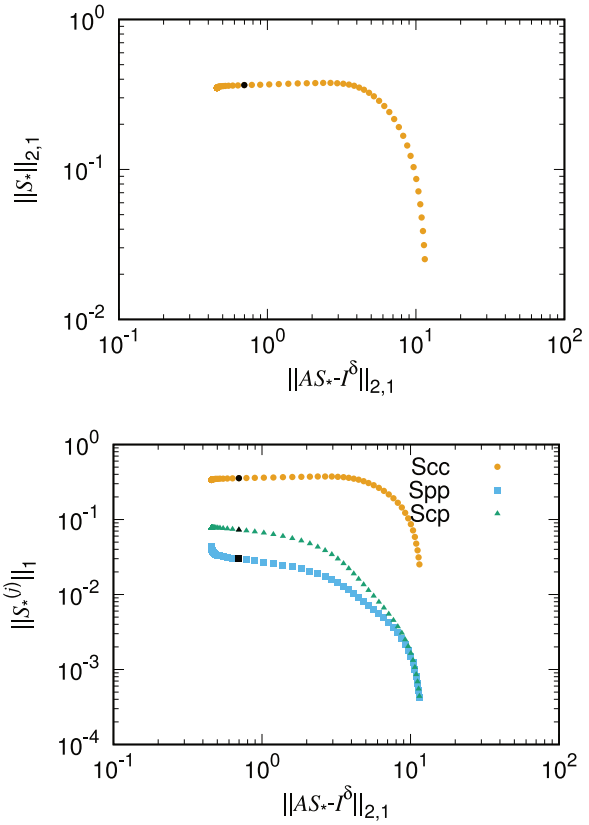

Fig. 7 Reconstructed $\| S_*^{(j)} \|_1$ ($j = 1, 2, 3$) are plotted as functions of $\| A\mathbf{S}_\alpha^\delta - \mathbf{I}^\delta \|_{2,1}$. Solid black circles for S_{CC}, S_{PP} and S_{CP} show the points for $\alpha = 20$. Here, $S_*^{(1)} = S_{PP,*}$, $S_*^{(2)} = S_{CC,*}$ and $S_*^{(3)} = S_{CP,*}$

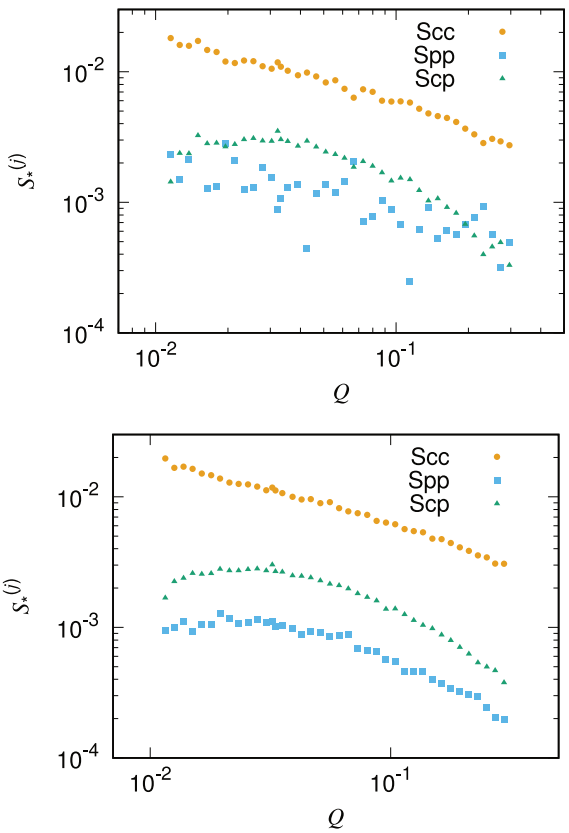

Fig. 8 (Top) Reconstructed $S_{CC,*}$, $S_{PP,*}$ and $S_{CP,*}$ are plotted against Q_i ($i = 1, \ldots, N_Q$) for $\alpha = 0$ (no regularization). (Bottom) Reconstructed $S_{CC,*}$, $S_{PP,*}$ and $S_{CP,*}$ are plotted against Q_i ($i = 1, \ldots, N_Q$) for $\alpha = 20$ and $L = \mathrm{diag}(1,\ 0.1,\ 1)$. Here, $S_*^{(1)} = S_{PP,*}$, $S_*^{(2)} = S_{CC,*}$ and $S_*^{(3)} = S_{CP,*}$

Figs. 9 and 10, the reconstruction is not successful for $A^{(123)}$, while good reconstruction results are obtained for $A^{(456)}$. In both Figs. 9 and 10, α is set to (left) 0, (center) 10, and (right) 20; the matrix L is set to $L = \mathrm{diag}(1, 0.1, 1)$ for all panels. In Fig. 11, the reconstructions obtained for $A^{(123)}$ and $A^{(456)}$ with $\alpha = 10$ are compared with the reconstruction for A with $\alpha = 20$, which is shown in Fig. 8 (bottom). It is seen that even if $m < 8$, good reconstruction effects can be achieved via regularization unless the condition number is extremely large.

Conclusions

The reason that an unstable reconstruction is obtained for $\mathbf{S}$ with the naive use of SVD is that singular values of the matrix A are not on the same order. As seen in this paper, the Tikhonov regularization term can stabilize the solution of the inverse problem.

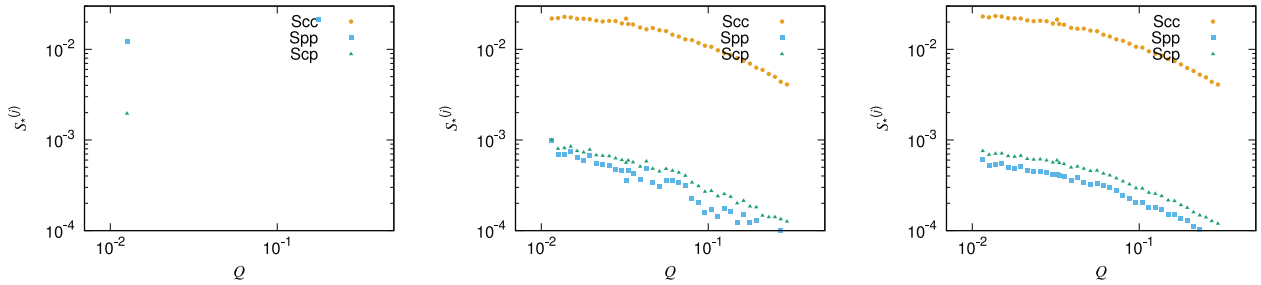

Fig. 9 Reconstructed $S_{\mathrm{CC},*}$, $S_{\mathrm{PP},*}$ and $S_{\mathrm{CP},*}$ are plotted against Q_i $(i = 1, \ldots, N_Q)$ for $A^{(123)}$ with (Left) $\alpha = 0$ (no regularization), (Center) $\alpha = 10$, and (Right) $\alpha = 20$. In all cases, $L = \mathrm{diag}(1, 0.1, 1)$. Here, $S_*^{(1)} = S_{\mathrm{PP},*}$, $S_*^{(2)} = S_{\mathrm{CC},*}$ and $S_*^{(3)} = S_{\mathrm{CP},*}$

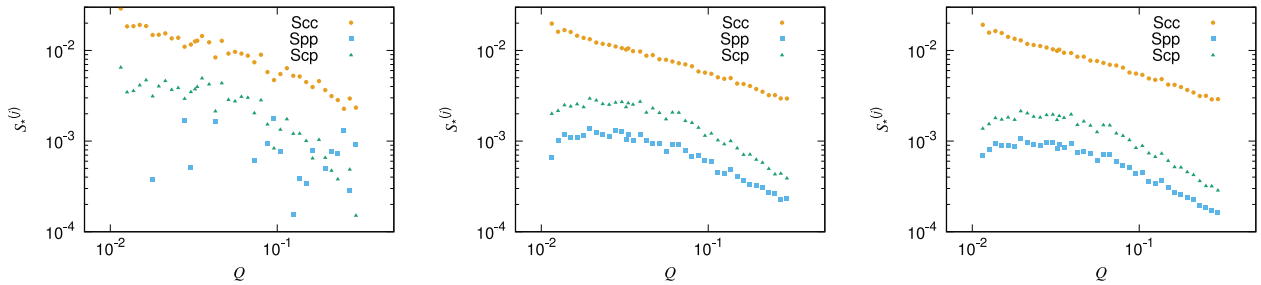

Fig. 10 Same as Fig. 10 but $A^{(456)}$ was used

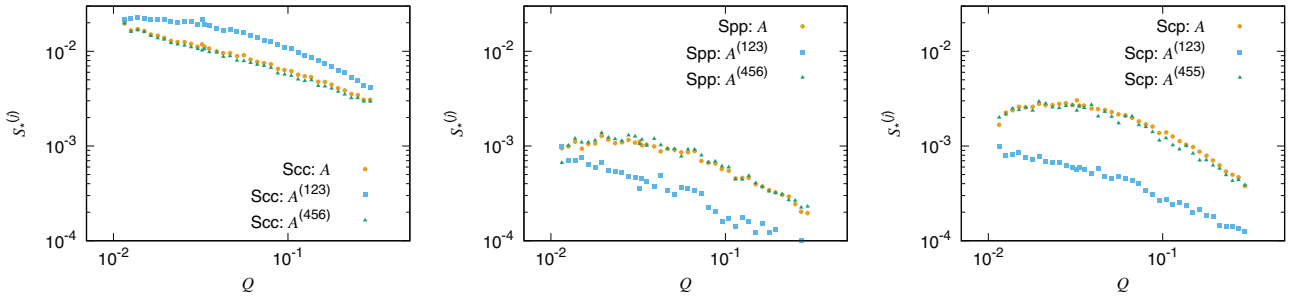

Fig. 11 Reconstructed $S_{\mathrm{CC},*}$, $S_{\mathrm{PP},*}$ and $S_{\mathrm{CP},*}$ for $m = 6$. For the reconstruction, the same parameters in Figs. 9 and 10) were used. For upper six intensities, the data for d-PR solutions $\varphi_{\mathrm{d}} = 0.90$ and $\varphi_{\mathrm{d}} = 0.85$ in Fig. 1b were not used. For lower six intensities, the data for h-PR solutions $\varphi_{\mathrm{d}} = 1$ and $\varphi_{\mathrm{d}} = 0.90$ in Fig. 1b were not used

The calculation presented in the previous section implies the procedure of reconstructing partial scattering functions. The reconstruction can done as follows.

- *Step 1*. First, $\mathbf{s} = \mathbf{S}$, and $B = A$ $(L = E)$ in (6). We calculate $\mathbf{s}_*$ in (23) and obtain a figure that is similar to Fig. 2 (top).
- *Step 2*. Utilizing the above result, the diagonal elements of L can be determined. Different choices of L are possible, but the elements of $\mathbf{s}_*$ possess the same order. The introduction of L is important, but the choice of L is not sensitive to the final result of $\mathbf{S}_*$.
- *Step 3*. Set $\mathbf{s} = L\mathbf{S}$, $B = AL^{-1}$ in (6).
- *Step 4*. The inverse problem $B\mathbf{s} = \mathbf{I}^{\delta}$ is solved via SVD, as shown in (23), (24). Thus, we obtain $\mathbf{s}_*$ for different values of α.
- *Step 5*.$\alpha > 0$ is obtained by plotting the graphs of $\|\mathbf{S}_*\|_{2,1}$ and $\| S_*^{(j)} \|_1$ $(j = 1, 2, 3)$ against $\|A\mathbf{S}_* - \mathbf{I}^{\delta}\|_{2,1}$ as is done in Figs. 4 and 7. We can pick an α for which $\|AS_* - I^{\delta}\|_{2,1}$ is small and the change exhibited by $\| S_*^{(j)} \|_1$ is small with respect to $\|AS_* - I^{\delta}\|_{2,1}$. More intuitively, we can choose a small $\alpha > 0$ within the the interval on which $\mathbf{s}_*$ is almost independent relative to α. We note that the reconstructed results should not be sensitive to the choice of α.

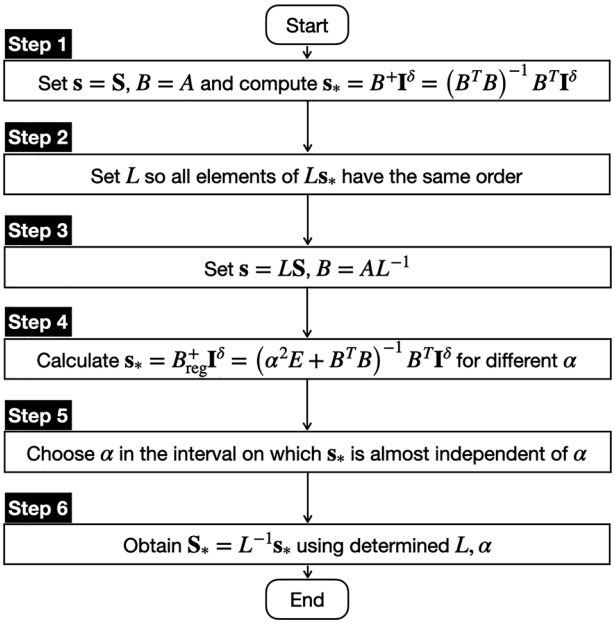

Fig. 12 Flowchart to obtain the reconstructed result $\mathbf{S}_*$ from the matrix A and measured data $\mathbf{I}^\delta$

- *Step 6*.$\mathbf{s}_*$ in (23) is calculated using the determined L and α. Then, we obtain $\mathbf{S}_* = L^{-1}\mathbf{s}_*$.

The above procedure is summarized in the flowchart presented in Fig. 12. In the above procedure, it is usually not difficult to determine α, L_1, L_2, and L_3 because the reconstructed results are not sensitive to the choices of α and L if they are properly chosen.

Although 3-component systems are assumed in this paper and A is an $m \times 3$ matrix, the regularization scheme can be readily applied to general p-component systems with an $m \times p$ matrix A.

Acknowledgements This research was initiated at the 7th JST workshop on unsolved problems (Morioka, Japan, 2023), which is greatly appreciated. The SANS experiment was carried out by the JRR-3 general user program managed by the Institute for Solid State Physics, The University of Tokyo (Proposal No. 7607).

Funding Second author: JST FOREST Program (JPMJFR2120).

Compliance with ethical standards

Conflict of interest The authors declare no competing interests.

References

1. Higgins, J.S., Benoit, H.C. Polymers and neutron scattering. Oxford University Press, 1998.
2. Richter D, Schneiders D, Monkenbusch M, Willner L, Fetters LJ, Huang JS. Polymer aggregates with crystalline cores: the system polyethylene-poly(ethylenepropylene). Macromolecules. 1997;30:1053–68.
3. Endo H, Miyazaki S, Haraguchi K, Shibayama M. Structure of nanocomposite hydrogel investigated by means of contrast variation small-angle neutron scattering. Macromolecules. 2008;41:5406–11.
4. Takenaka M, Nishitsuji S, Amino N, Ishikawa Y, Yamaguchi D, Koizumi S. Structure analyses of swollen rubber-filler systems by using contrast variation SANS. Macromolecules. 2009;42:308–11.
5. Jeffries CM, Graewert M.A., Blanchet C.E., Langley D.B., Whitten A.E., Svergun DI. Preparing monodisperse macromolecular samples for successful biological small-angle X-ray and neutron-scattering experiments. Nat Protoc. 2016;11:2122–53.
6. Mayumi K, ndo H, Osaka N, Yokoyama H, Nagao M, Shibayama M, Ito K Mechanically interlocked structure of polyrotaxane investigated by contrast variation small-angle neutron scattering. Macromolecules. 2009;42:6327–9.
7. Endo H, Mayumi K, Osaka N, Ito K, Shibayama M. The static structure of polyrotaxane in solution investigated by contrast variation small-angle neutron scattering. Polym J. 2011;43:155–63.
8. Mayumi K, Oda T, Miyajima S, Obayashi I, Tanaka K. Error evaluation of partial scattering functions obtained from contrast-variation small-angle neutron scattering. J Appl Crystallogr. 2025;58:4–17.
9. Obayashi I, Miyajima S, Tanaka K, Mayumi K. Enhanced estimation method for partial scattering functions in contrast variation small-angle neutron scattering via Gaussian process regression with prior knowledge of smoothness. J Appl Crystallogr. 2025;58:976–91.
10. Colton, D, Kress, R. Inverse Acoustic and Electromagnetic Scattering Theory. 2nd ed. Springer, 1998.
11. Engl, H.W., Hanke, M., Neubauer, A. Regularization of Inverse Problems. Kluwer Academic Publishers, 1996.
12. Hansen, P.C. The L-curve and its use in the numerical treatment of inverse problems. Computational Inverse Problems in Electrocardiology ed Johnston P. 119–42 WIT Press, 2001.